Molecular Cell, *Volume 47*

Supplemental Information

Independence of Repressive Histone Marks and Chromatin Compaction during Senescent Heterochromatic Layer Formation

Tamir Chandra, Kristina Kirschner, Jean-Yves Thuret, Benjamin D. Pope, Tyrone Ryba, Scott Newman, Kashif Ahmed, Shamith A. Samarajiwa, Rafik Salama, Thomas Carroll, Rory Stark, Rekin's Janky, Masako Narita, Lixiang Xue, Agustin Chicas, Sabrina Nũnez, Ralf Janknecht, Yoko Hayashi-Takanaka, Michael D. Wilson, Aileen Marshall, Duncan T. Odom, M. Madan Babu, David P. Bazett-Jones, Simon Tavaré, Paul A.W. Edwards, Scott W. Lowe, Hiroshi Kimura, David M. Gilbert, Masashi Narita

SUPPLEMENTAL EXPERIMENTAL PROCEDURES

Cell Culture and Viral Infections, and antibodies

IMR90 human diploid fibroblasts (ATCC) were cultured in DMEM supplemented with 10% FBS and antibiotics in 5% oxygen (Young et al., 2009). The following vectors were used for retroviral or lentiviral gene transfer: pLNCX2 (ER: H-*ras*V12) (Young et al., 2009), pBabe-puro (H-*ras*V12 and *MEK1* Q56P), pLPC (*GFP-M33*), pWZL-Hygro (*p16*), pQCXIH (*HA-JMJD2D* and its H192A mutant) (Shin and Janknecht, 2007), pSin-miR30-puro (sh-HMGA1), pMSCV-miR30-puro (sh-HMGA1, sh-Rb and sh-SUZ12), pSIN-puro (sh-p400), Lentiviral miR30 (sh-HMGA1 and sh-Rb).

The following antibodies were used for immunofluorescence: anti-H3K36me3 (abcam ab9050), anti-H3K4me3 (abcam ab8580 or clone CMA304) (Kimura et al., 2008), anti-H3K27me3 (clone CMA323) (Hayashi-Takanaka et al., 2011), anti-H3K9me3 (Millipore 07-442 or clone CMA318) (Hayashi-Takanaka et al., 2011), anti-H3K9me2 (clone CMA317) (Hayashi-Takanaka et al., 2011), anti-BrdU (Pharmingen). The CENPA and H3K9me2/3 antibodies were generous gifts from A. Straight (Stanford University School of Medicine) and D. Reinberg (New York University Medical School), respectively. Following antibodies were used for immunoblotting: anti-p16 (Santa Cruz sc-759) and anti-Ras (Santa Cruz sc-29), anti-CCNA2 (Sigma C4710) and anti-β-actin (Sigma A5441), anti-H3K9me3 (clone CMA318), anti-H3K27me3 (clone CMA323), and anti-SUZ12 (Abcam 12073). ChIPs for deep sequencing were performed using specific antibodies against histone modifications H3K4me3 (clone CMA304), H3K9me3 (clone CMA318), H3K9me2 (clone CMA317), H3K27me3 (clone CMA323 and Upstate 07-449), and H3K36me3 (clone CMA333) (Rechtsteiner et al., 2010).

Immunofluorescence and Fluorescence In Situ Hybridization (FISH)
Immunofluorescence was performed according to standard procedures (Narita et al., 2003). For GFP-M33 expressing cells, a pre-extraction step was added before fixation (Figure S1D). Cells on coverslips were incubated in 0.3 mg/ml digitonin (Sigma)/CSK buffer on ice for 5min, then fixed by paraformaldehyde for 15 min at room temp. No pre-extraction step was added for other Immunofluorescence samples.

FISH was performed as described in (Solovei et al., 2002), with the addition of a pre-extraction step before fixation. Whole chr X paint was generated as described previously (Telenius et al., 1992). X-alpha satellite FISH was performed using the probe pDMX1 as shown (Archidiacono et al., 1995).

RNAi target sequences
The following target sequences were used to construct miR30 based shRNAs: gcaaatggatttagtgaaatt for sh-SUZ12; gcctgggatctgagtacatat for sh-HMGA1 (Narita et al., 2006), and gcagttcgatatctactgaaa for sh-Rb (Chicas et al., 2010). Sh-p400 was described previously (Chan et al., 2005).

ELISA
ELISA was performed as previously described (Kimura et al., 2008). Microtiter plates coated with the peptides were incubated with 3-fold dilutions of CMA318 hybridoma culture supernatant in PBS, starting from 1:100 dilution. After incubation with peroxidase-conjugated secondary antibody and washing, the colorimetric signal of tetramethylbenzidine was detected by measuring the absorbance at 405 nm (Abs) using a plate reader.

Live Cell Imaging of Replication Foci
Two days after the administration of 4-OHT, ER:Ras expressing IMR90 cells were loaded with Alexa488-dUTP (Invitrogen; 5 μl; 50 μM) and then Cy3-dUTP (Perkin-Elmer; 5 μl; 50 μM) for four hours each using a bead-loading method, as described previously (Manders et al. 1999). Live cell imaging was started at 3.5 h after the loading of Cy3-dUTP using an inverted microscope (Ti-E; Nikon) with a PlanApo VC 60× (NA = 1.2) water-immersion objective lens with Immersol W (Carl Zeiss). Alexa488 and Cy3 fluorescence images were collected every 30 min. To chase the cell movements, a large area spanning ~930×800 μm^2 (7×6 image frames) was collected.

Gene Expression
Immunoblotting was carried out as described (Narita et al., 2006). For microarray experiments, total RNAs were isolated from ER:Ras IMR90 cells with (RIS) or without (growing) 4OHT at day 6. cRNA was hybridized to Human-6 v2 Expression BeadChips (Illumina). Five biological replicates were

performed for each experimental condition (Young et al., 2009).

Statistical Analysis

Statistical differences between experimental groups were analyzed using two-tailed Student's t tests.

ChIP-Seq Analysis

Sequences were processed by the Illumina analysis pipeline version 1.6.1, and aligned to the Human Reference Genome (assembly hg18, NCBI Build36.1, March 2008) using BWA version 0.5.5 (Li and Durbin, 2009). Reads were filtered by removing those with a BWA alignment quality score less than 15. Total read counts for all samples are summarized in Tables S1 and S2. For the calculation of the proportions of total reads within genomic features, transcript information was retrieved from the UCSC Ensembl gene definitions for the hg18 genome assembly. Gene boundaries were defined from Ensembl known transcripts as the beginning and end of the first and last gene exons respectively and promoter regions as 5Kb upstream from these defined transcription start sites. Numbers of reads aligning to these regions were calculated using Rsamtools and reads aligning to overlapping promoter and genic regions assigned to promoter regions. The overlapping percentage was also confirmed using RSEG (Song and Smith, 2011). RSEG was used as previously described with mode 2, to identify regions significantly enriched for histone marks across the genome. Dead zones file across NCBI Build 36.1 genome for 36 read length is used to eliminate false positive regions (Song and Smith, 2011).

For Figures 3B-3E, genomic intervals were either fixed-size windows (20Kb, 50Kb, 100Kb, 500Kb, and 1,000Kb) over the whole genome, or fixed-size windows relative to transcription start sites 500b upstream and 5Kb downstream of each TSS. Any overlapping intervals were merged. For each sample, a RPKM score (Mortazavi et al., 2008) was derived for each interval. Intervals that did not have a read density of at least 1RPKM in at least one sample were eliminated (except for the 1,000Kb windows, where all read densities were included regardless of RPKM). Clustering and correlation heat maps were derived by taking the Pearson correlation coefficient of the RPKM values for all active intervals for each pair of samples.

Identification of intervals with significantly different levels of enrichment between Growing and Senescent cells was performed using the Bioconductor package DiffBind (http://bioconductor.org/packages/release/bioc/html/DiffBind.html).

Chromosome-wide Landscapes

Chromosome-wide landscapes of repressive marks were computed based on the read depth at each position of the genome. If not stated otherwise, these were binned into 1Kb bins with a rolling mean of 1000. After binning, the intensities were normalized to the total number of reads per chromosome. For the genome wide RT data, no smoothing was applied. For correlations between chromosome-wide landscapes, Spearman's rank correlation coefficient was calculated. Regions without any signal after binning and smoothing that identify non-annotated and centromeric stretches were filtered out. A rolling mean of 200 showed similar results (data not shown).

Hilbert Curve Visualization

Hilbert Curve Visualization (HCV) of ChIP-Seq data was generated using the ShortRead (Morgan et al., 2009) and HilbertVis and HilbertVisGUI (Anders, 2009) R/Bioconductor tools (Gentleman et al., 2004). The Hilbert plots represent linear sequence data visualized in two-dimensional space, where each colored spot is a peak. The area of each colored region in the two-dimensional plot is proportional to the width of the peak, and the intensity of the spot corresponds to the height of the peak. Regions within the image were further magnified either 4 fold or 64 fold for detailed study of specific chromosomal regions. RefSeq transcript annotation for chromosome 9 was obtained from the UCSC genome browser (Rhead et al. 2010). Two colour overlay plots were generated using Adobe Photoshop 'darkened' function, where overlapping spots are darkened.

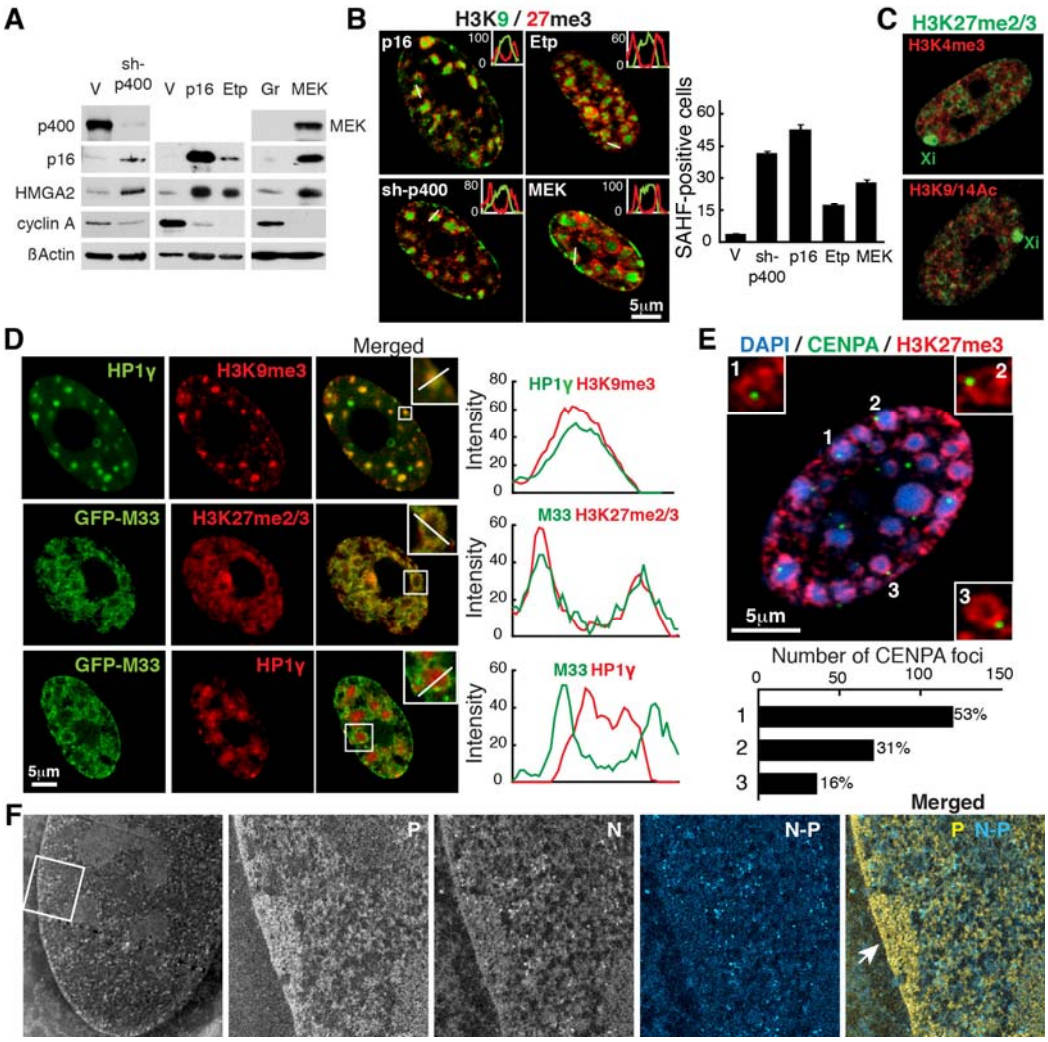

Figure S1. Characterization of SAHF, Related to Figure 1

(A and B) Senescence was induced by various methods in IMR90 cells, such as overexpression of p16 and MEK1 Q56P (MEK), sh-p400, and DNA damage (Etp). DNA damage was induced by a 48-h Etoposide (100 μM) treatment (Etp) and cells were harvested 5 days after the removal of the drug. V, corresponding vector control; Gr, growing (A). Cells were assessed for the proteins indicated by Immunoblotting (A) and SAHF formation by confocal microscopy (B). Insets show intensity profiles along the indicated line (B). Data are mean ± SEM (B).

(C) Representative confocal images for indicated histone marks in RIS IMR90 cells. The ring structure was also obtained using anti-H3K27me2/3 (Sarma et al., 2004).

(D) Representative confocal images for the indicated proteins and histone marks in RIS IMR90 cells. The regions indicated by the rectangles are magnified in the insets. Fluorescence intensity profiles along the lines in the insets are shown (right). For cells expressing GFP-M33 (mouse Pc1), cells

were pre-extracted before fixation to remove the superfluous signal derived from the chromatin unbound faction of GFP-M33.
(E) Representative confocal image of CENPA and H3K27me3 in RIS. 1, 2 and 3 show three representative SAHFs with distinct CENPA locations used to classify CENPA positions within a single SAHF. Frequency of each pattern is shown.
(F) Electron Spectroscopic Imaging (ESI) of growing IMR90 cells as in Figure 1F. The arrow indicates a peri-nuclear heterochromatic region (‘peri’ in Figure 1F). Small bright round objects represent gold particles labelling H3K27me3, which are most obvious in the panel, N-P.

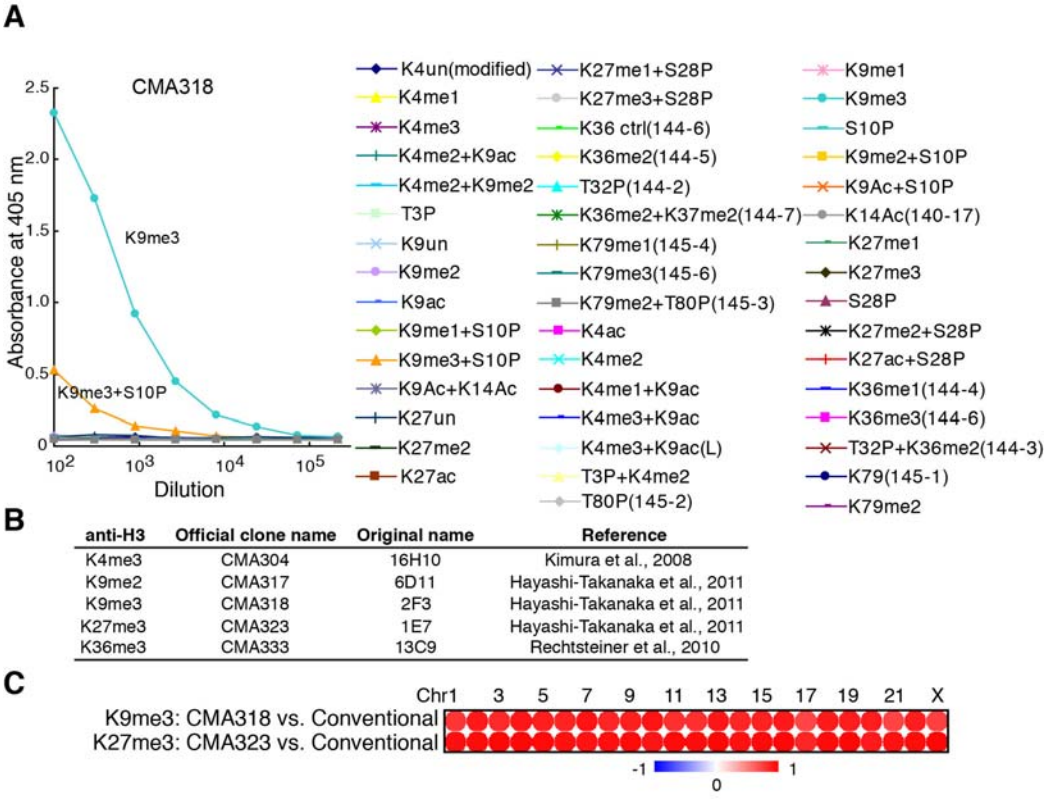

anti-H3	Official clone name	Original name	Reference
K4me3	CMA304	16H10	Kimura et al., 2008
K9me2	CMA317	6D11	Hayashi-Takanaka et al., 2011
K9me3	CMA318	2F3	Hayashi-Takanaka et al., 2011
K27me3	CMA323	1E7	Hayashi-Takanaka et al., 2011
K36me3	CMA333	13C9	Rechtsteiner et al., 2010

Figure S2. Specificity of the Monoclonal Antibodies Used in This Study, Related to Figure 3

(A) The specificity of the monoclonal antibody against H3K9me3, clone CMA318, was tested against a panel of modified peptides by ELISA.

(B) List of additional information on the monoclonal antibodies used in this study.

(C) Graphical representation of chromosome-wide Spearman correlations between ChIP-seq data generated by different antibodies are shown as in Figure 4A. Our representative data for each K9me3 (with CMA318) and K27me3 (with CMA323) in growing IMR90 cells were compared to publicly available data using conventional antibodies in the same cells (Hawkins et al. 2010).

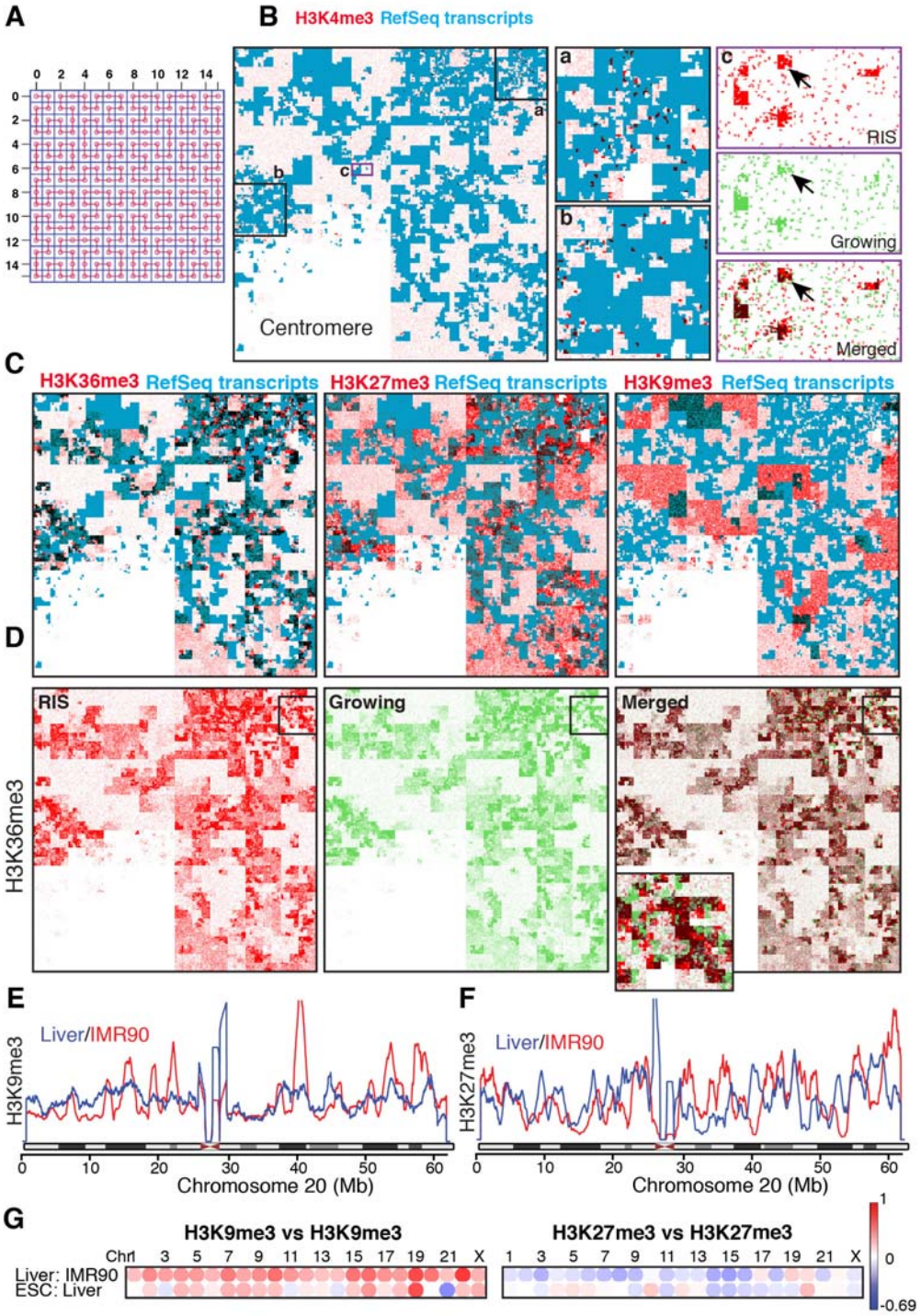

Figure S3. Visualization of ChIP-Seq Data with the Hilbert Curve, Related to Figure 4

(A) The Hilbert curve is a continuous fractal space-filling curve constructed in a recursive manner. The fourth step in Hilbert curve construction is shown.

(B and C) Association between transcription (RefSeq transcripts) and H3K4me3 (B), H3K36me3, H3K27me3, or H3K9me3 (C). ChIP-seq data for these marks (red) on chr 9 in IMR90 cells are visualized using the Hilbert

curve. RefSeq transcripts (Blue) are overlaid using Photoshop blending mode ‘darken’. Two gene rich areas (a and b) are magnified to show the correlation between H3K4me3 ‘puncta’ and RefSeq transcripts. The region (c) including the *p16INK4A* locus (arrow) is also magnified, indicating the enrichment of H3K4me3 upon this locus in RIS cells.
(D) Substantial differences in H3K36me3 pattern between growing and RIS cells. The regions indicated by rectangles are magnified. Photoshop blending mode ‘darken’ was used for the overlays.
(E-G) Cross-lineage comparison of H3K9me3 (E) or H3K27me3 (F) landscape between human liver and IMR90 cells on chr 20. (G) Graphical representation of chromosome-wide relationship between cells indicated for each H3K9me3 and H3K27me3. Liver, human liver (male) from this study; ESC, human ESCs (Hawkins et al., 2010). We estimate ~80% of DNA isolated from the liver tissue is hepatocyte in origin (Schmidt et al. 2009). Following local research ethics committee approval, normal human liver was obtained from a 56-year old male who had undergone partial liver resection for colorectal cancer metastasis.

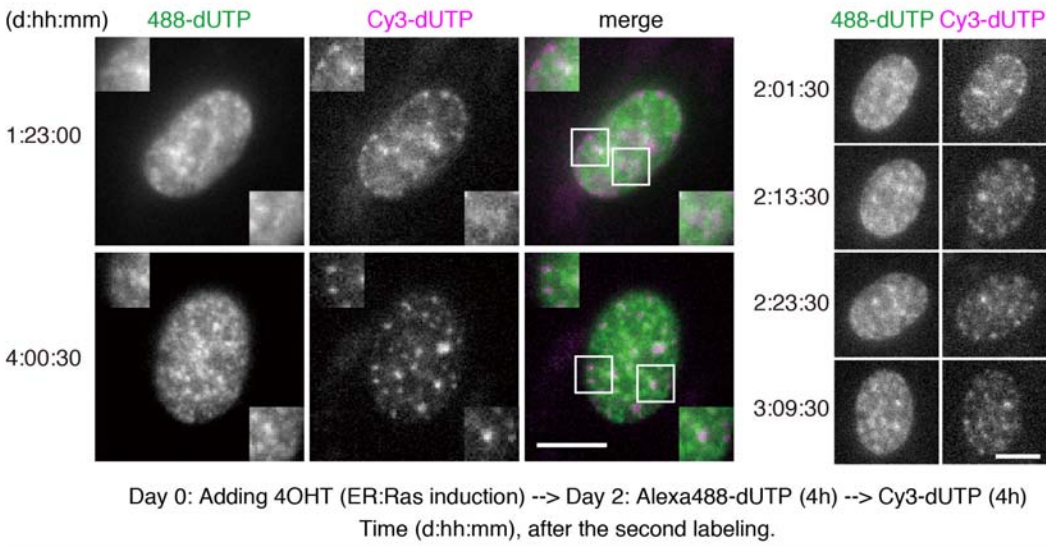

Figure S4. Time-Lapse Imaging of Replication Timing during RIS, Related to Figure 5

Cells were sequentially labelled by Alexa488-dUTP and Cy3-dUTP for 4h each, using the beads loading technique, and then monitored during SAHF formation. Representative images of the same nucleus before and after SAHF formation are shown (left). Images between these two time points are shown in the right panel. To capture the last S-phase before senescence establishment, we labelled cells two days after 4-OHT treatment, when some cells are still proliferating. Insets show magnifications of the regions indicated by the rectangles. Time stamps (d:hh:mm) refer to time after the second labeling.

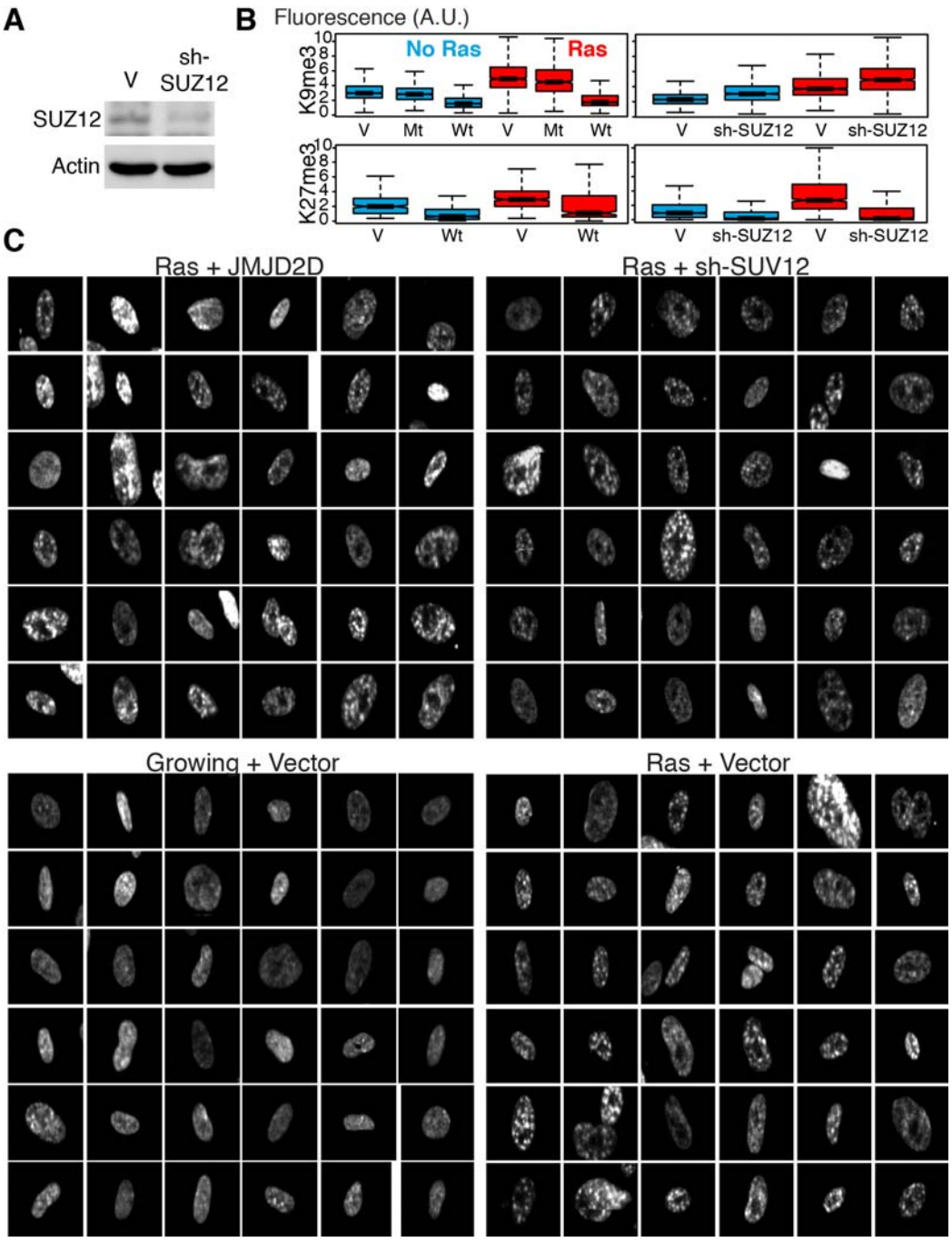

Figure S5. Depletion of Repressive Mark H3K9me3 or H3K27me3 Does Not Prevent SAHF Formation, Related to Figure 7

(A) Immunoblotting for indicated proteins in IMR90 cells expressing sh-SUZ12 and control vector (V).

(B) Distribution of fluorescence intensity (integrated value over the area of the nucleus) for the indicated histone marks in single cells, as measured by laser scanning cytometry. ER:Ras-expressing cells were infected with retroviruses

expressing either wild type (Wt) JMJD2D or its catalytic inactive mutant (Mt), or sh-SUZ12, and then ER:Ras was induced by 4OHT as in Figure 7.
(C) DAPI staining pattern of panels of cells selected from the cell populations indicated. 36 cells were chosen from the lowest 20% intensity for each mark, while control cells (‘Growing+Vector’ or ‘Ras+Vector’) were randomly chosen from each population. SAHF formation is evident in those cells with the lowest amount of each repressive mark.

Table S1. Summary of ChIP-Seq Reads for Histone Marks in Growing (Gr) and Ras-Induced Senescent (RIS) IMR90 Cells, Related to Figure 3

Marks (H3-)	Cells	Number of Replicates	% Reads in Genes	% Reads in Promoters	% Reads in intergenic Regions
K9me3	Gr	2	30.7 (21.3)	4.8 (3.1)	64.4 (75.6)
K9me3	RIS	2	31.9 (21.4)	5.1 (3.0)	63.0 (75.6)
K9me2	Gr	3	35.7 (21.7)	6.1 (3.4)	58.3 (74.9)
K9me2	RIS	3	37.2 (28.4)	6.0 (5.0)	56.8 (66.6)
K27me3	Gr	2	36.4 (31.7)	8.5 (9.5)	55.1 (58.8)
K27me3	RIS	3	37.3 (31.5)	7.6 (8.1)	55.2 (60.4)
K36me3	Gr	2	69.9 (79.1)	8.2 (10.4)	22.0 (10.5)
K36me3	RIS	2	67.8 (78.6)	7.6 (9.7)	24.6 (11.7)
K4me3	Gr	2	46.9 (39.3)	18.8 (28.7)	34.3 (32.0)
K4me3	RIS	3	48.6 (43.0)	23.3 (34.7)	28.2 (22.3)

The mean percentage of total sequence reads mapped to genic (Genes), promoter and intergenic regions are shown for each histone mark and condition indicated. Promoter regions were defined as 5Kbp regions upstream of transcription start site. The numbers of biological replicates for each histone mark and condition group pair are shown. Reads within overlapping promoter and genic regions were assigned to promoter regions in calculation of percentages. Reads were assigned as intergenic if they were not mapped to either genic or promoter regions. Individual data sets can be found in Table S2. Data obtained using RSEG are shown in parentheses for comparison.

SUPPLEMENTAL REFERENCES

Archidiacono, N., Antonacci, R., Marzella, R., Finelli, P., Lonoce, A., and Rocchi, M. (1995). Comparative mapping of human alphoid sequences in great apes using fluorescence in situ hybridization. Genomics *25*, 477–484.

Chan, H.M., Narita, M., Lowe, S.W., and Livingston, D.M. (2005). The p400 E1A-associated protein is a novel component of the p53 --> p21 senescence pathway. Genes Dev. *19*, 196-201.

Chicas, A., Wang, X., Zhang, C., Mccurrach, M., Zhao, Z., Mert, O., Dickins, R. A., Narita, M., Zhang, M., and Lowe, S. W. (2010). Dissecting the unique role of the retinoblastoma tumor suppressor during cellular senescence. Cancer Cell *17*, 376–387.

Gentleman, R.C., Carey, V.J., Bates, D.M., Bolstad, B., Dettling, M., Dudoit, S., Ellis, B., Gautier, L., Ge, Y., Gentry, J.*, et al.* (2004). Bioconductor: open software development for computational biology and bioinformatics. Genome Biol. *5*, R80.

Hayashi-Takanaka, Y., Yamagata, K., Wakayama, T., Stasevich, T.J., Kainuma, T., Tsurimoto, T., Tachibana, M., Shinkai, Y., Kurumizaka, H., Nozaki, N., *et al*. (2011). Tracking epigenetic histone modifications in single cells using Fab-based live endogenous modification labeling. Nucleic Acids Res. 39, 6475-6488.

Kimura, H., Hayashi-Takanaka, Y., Goto, Y., Takizawa, N., and Nozaki, N. (2008) The organization of histone H3 modifications as revealed by a panel of specific monoclonal antibodies. Cell Struct. Funct. *33*, 61-73.

Li, H., and Durbin, R. (2009). Fast and accurate short read alignment with Burrows-Wheeler transform. Bioinformatics *25*, 1754–1760.

Manders, E.M., Kimura, H. and Cook, P.R. (1999) Direct imaging of DNA in living cells reveals the dynamics of chromosome formation. J. Cell Biol. *144*, 813-821.

Morgan, M., Anders, S., Lawrence, M., Aboyoun, P., Pages, H., and Gentleman, R. (2009). ShortRead: a bioconductor package for input, quality assessment and exploration of high-throughput sequence data. Bioinformatics *25*, 2607-2608.

Mortazavi, A., Williams, B. A., McCue, K., Schaeffer, L., and Wold, B. (2008). Mapping and quantifying mammalian transcriptomes by RNA-Seq. Nat. Meth. *5*, 621–628.

Rechtsteiner, A., Ercan, S., Takasaki, T., Phippen, T.M., Egelhofer, T.A., Wang, W., Kimura, H., Lieb, J.D., and Strome, S. (2010). The Histone H3K36

Methyltransferase MES-4 Acts Epigenetically to Transmit the Memory of Germline Gene Expression to Progeny. PLoS Genet. 6, e1001091

Rhead, B., Karolchik, D., Kuhn, R.M., Hinrichs, A.S., Zweig, A.S., Fujita, P.A., Diekhans, M., Smith, K.E., Rosenbloom, K.R., Raney, B.J.*, et al.* The UCSC Genome Browser database: update 2010. Nucleic Acids Res. *38*, D613-619.

Sarma, K., Nishioka, K., and Reinberg, D. (2004). Tips in analyzing antibodies directed against specific histone tail modifications. Meth. Enzymol. *376*, 255–269.

Schmidt, D., Wilson, M.D., Spyrou, C., Brown, G.D., Hadfield, J., and Odom, D.T. (2009). ChIP-seq: using high-throughput sequencing to discover protein-DNA interactions. Methods *48*, 240-248.

Solovei, I., Walter, J., Cremer, M., Habermann, F., Schermelleh, L. and Cremer, T. (2002). FISH on three-dimensionally preserved nuclei. In FISH, B. Beatty, S. Mai and J. Squire, ed. (Oxford, UK: Oxford University Press), pp. 119-157.

Telenius, H., Pelmear, A. H., Tunnacliffe, A., Carter, N. P., Behmel, A., Ferguson-Smith, M. A., Nordenskjöld, M., Pfragner, R., and Ponder, B. A. (1992). Cytogenetic analysis by chromosome painting using DOP-PCR amplified flow-sorted chromosomes. Genes Chromosom. Cancer *4*, 257–263.